Table S1. Elevation of upper and lower bounds of *Saccostrea cucullata* at rocky shores and tidal pools in Big Wave Bay, expressed in standardised water level index (SWLI) units and metre (m) relative to Hong Kong Principal Datum (mPD). Elevation in mPD is referenced to the tidal datums from the Tai Miu Wan tide gauge.

Geomorphic setting	***n***	***Lowest elevation***		***Highest elevation***		***Mean elevation***	
		SWLI units	mPD	SWLI units	mPD	SWLI units	mPD
Rocky shore	89	25	0.76	190	1.91	107	1.33
Tidal pool	70	169	1.76	267	2.45	210	2.05

Figure S1. Quantile-Quantile (QQ) plot comparing the quantiles of the observed data distribution to a theoretical normal distribution. The red line represents the expected quantiles under normality, and the dotted lines indicate the 95% confidence bounds. Data points falling close to the red line suggest that the data follows a normal distribution, while deviations, especially outside the confidence bounds, indicate potential departures from normality.

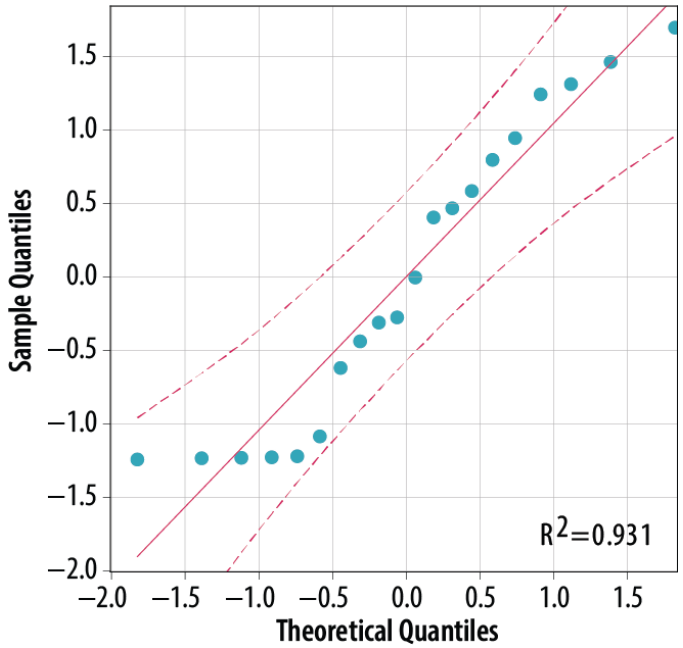

Figure S2. A) The regional distribution of S. cuccullata and their presence at surveyed sites in Hong Kong, along with the nearest tide gauge. B) Average relative abundance of S. cuccullata across 16 surveyed sites during the wet (blue bars) and dry seasons (orange bars).

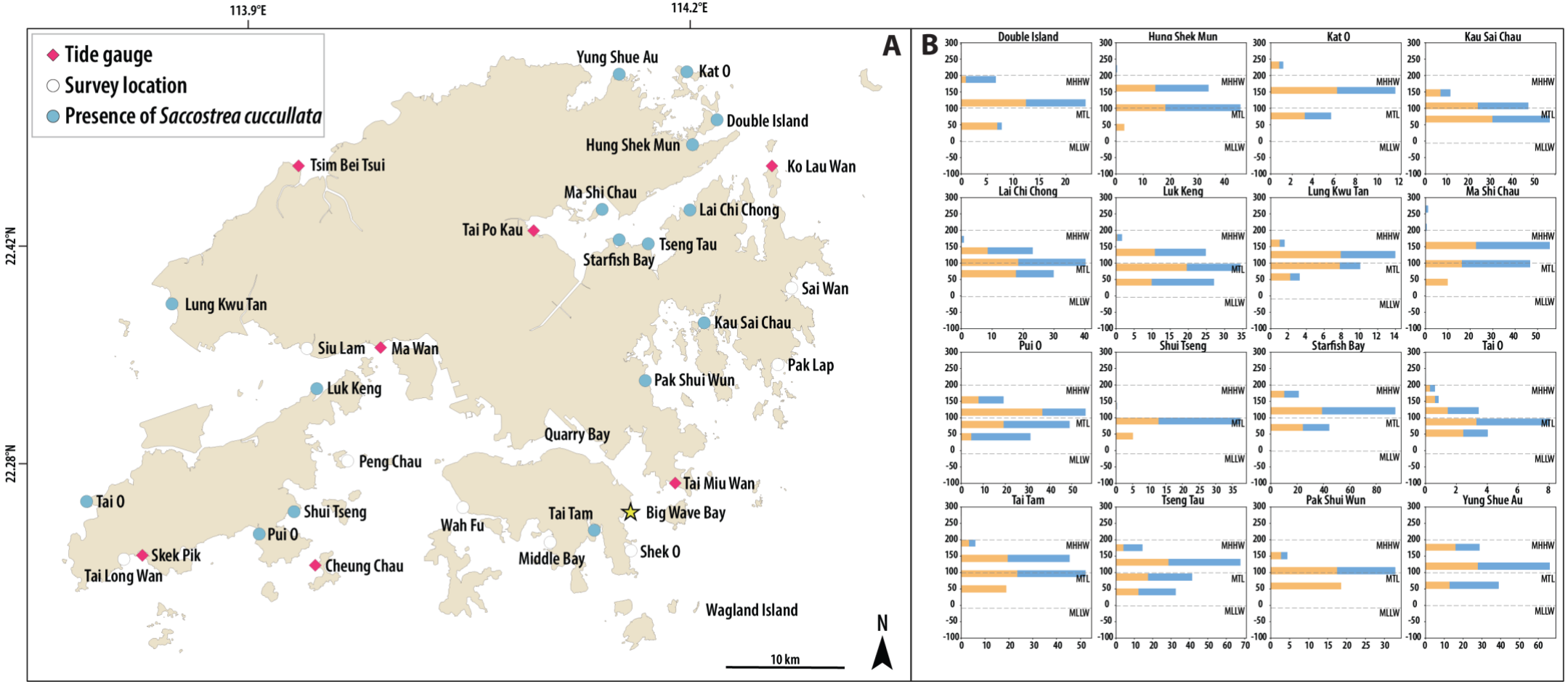

Table S2. Average relative abundance and vertical distribution of *Saccostrea cucullata* during wet and dry season in Hong Kong.

Season	***Lowest elevation (SWLI units)***	***Highest elevation (SWLI units)***	***Mean elevation (SWLI units)***	***Skewness***	***Average relative abundance(%)***
Wet	46	236	110	0.2	11.6
Dry	46	266	111	-0.001	13.7
Annual	46	266	111	0.1	12.7

Table S3. Tide level statistics and return periods corresponding to the lowest elevations of the LiDAR-derived oyster reef point cloud in Big Wave Bay. Data are sourced from the nearest two tide gauges: Tai Miu Wan (2004–2023) and Waglan Island (1999–2018)

Tide gauge	***Reading corresponding to minimum reef elevation***		***Average number of day / yr***	***Return period (year)***
	SWLI units	***mPD***		
Tai Miu Wan	320	2.85	0.095	10.5
Waglan Island	320	2.84	0.055	18.2

Figure S3. Ternary classification of reef types based on primary components: in-place skeletal structures, sedimentary matrices, and cement (Riding, 2012). At each apex, the respective component constitutes 100% of the reef structure, with its proportion gradually decreasing along lines that extend perpendicularly from each apex toward the opposite side, where the component is absent. A filled frame reef comprises approximately 30–70% in-place skeletal structures, 30-60% detrital matrix, and 0–30% cement. Frame reefs, cluster reefs, and segment reefs share similar compositional characteristics, though cluster reefs contain a lower proportion of skeletal material and a higher amount of detrital matrix. Estimated compositional fields occupied by the BWB oyster reef in skeleton–matrix–cement ternary diagram highlighted by cross line pattern.

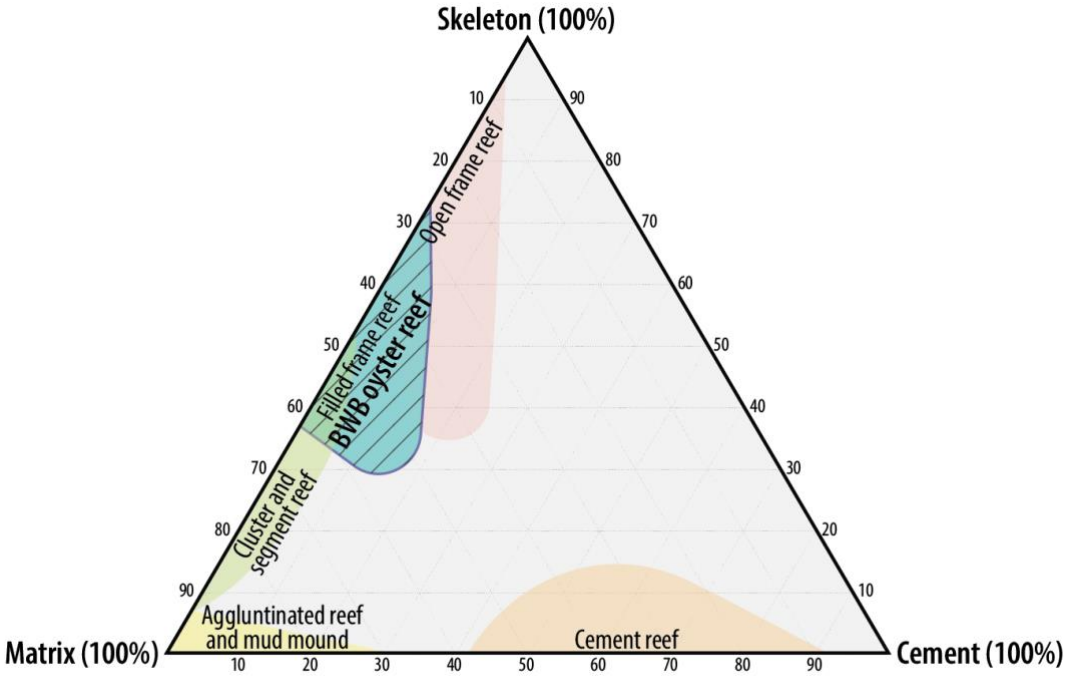

Figure S4. Roundness and circularity of sediment grains that formed matrix in the skeleton gravity (n = 50), with reference images of grains edited based on Krumbein and Sloss (1951).

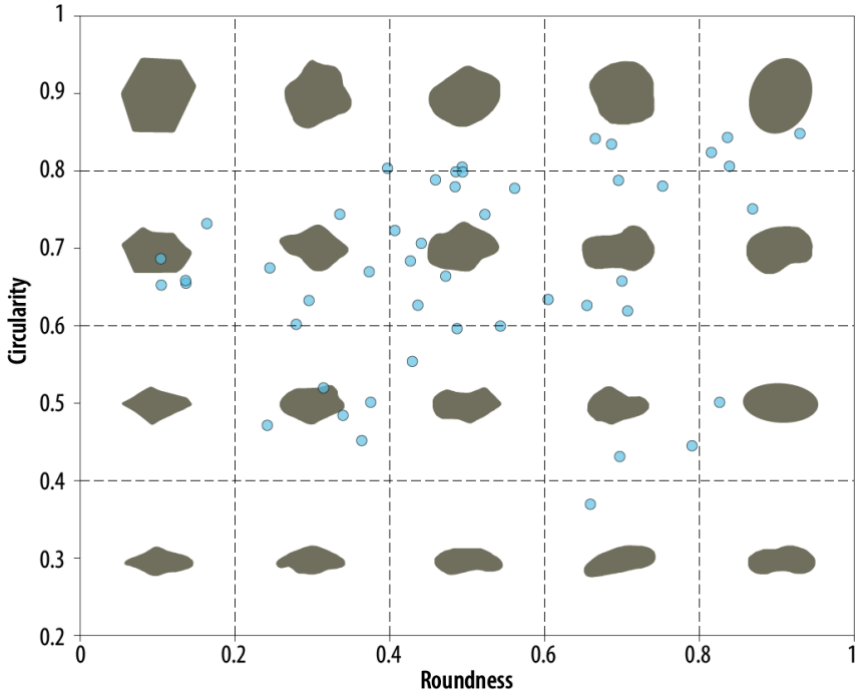

Following the approach of Takashimizu et al. (2016), we used ImageJ (Abràmoff et al. 2004; Schneider et al. 2012) to assess the roundness and circularity of sediment grains in the reef matrix. within a 5 x 5 mm grid (n = 50):

$$\text{Roundness} = \text{Circularity} + (\text{Circularity}_{\text{perfect}} - \text{Circularity}_{\text{aspect ratio}}), \quad \text{(S1)}$$

where $\text{Circularity}_{\text{perfect}}$ is the circularity of a perfect circle, and Circularity is defined by Cox (1927) as

$$\text{Circularity} = 4\pi\left(\frac{\text{area}}{\text{perimeter}^2}\right). \quad \text{(S2)}$$

The area, perimeter, $\text{Circularity}_{\text{aspect ratio}}$, and major axis length, and minor axis length of individual sediment grains were measured from the digital slide scans using ImageJ software. The roundness was scaled to Krumbein's Index (Krumbein, 1941) to allow comparison to other studies (Takashimizu et al., 2016).

Table S4. Indicative meaning used for the compilation of RSL data in Hong Kong and the PRD regions. The compilation followed international community standards of the HOLSEA protocol (https://www.holsea.org/) (Khan et al., 2019).

Indicator	***Facies***	***Supporting evidence***	***Reference water level***	***Indicative range***
	Tidal flat	**<u>Diagnostic criteria:</u>** <u>Macrofossil:</u> Presence of burrows from bivalves and articulated shells such as *Potamocorbula amurensis* (Asian brackish-water clam) and *Corbicula* spp. (Hori et al., 2004; Meacham, 1978), which are characteristic of muddy or sandy substrates in intertidal and brackish-water environments (Carlton et al., 1990). <u>Microfossil:</u> Diatom assemblage containing brackish and freshwater benthic diatom taxa, with brackish diatom (including planktonic type) >50% (Xiong et al., 2018a, 2018b; Xiong et al., 2020). <u>Sedimentary description:</u> Rhythmic sand–mud couplets, sand layers forms during ebb and flood currents, or mud drapes accumulated from suspension during or near tidal slack water. Bidirectional ripple cross lamination, which indicates influence of reversing tidal currents. (Tanabe et al., 2003; Hori et al., 2004; Tanabe er al., 2006).	(HAT+LAT)/2	HAT-LAT

	Mangrove	**<u>Diagnostic criteria:</u>** <u>Sedimentary description:</u> Mud to fine sandy mud that contains mangrove plant subfossils (often including leaf debris) (Huang 1986; Owen et al., 1998). <u>Microfossil:</u> Pollen assemblage containing >20% mangrove taxa (Zheng, 2000; Xia et al., 2019). <u>Geochemistry:</u> Bulk sediment $\delta^{13}C$ of -22.1 to -25.9‰, TOC of 2 to 7%, and C/N of 8 to 29 (Yu et al., 2010; Xia et al., 2019; Sun et al., 2021; Yu et al., 2025)	(HAT+MTL)/2	HAT-MTL
	Marine/delta front/estuarine deposit	**<u>Diagnostic criteria:</u>** <u>Sedimentary description:</u> Homogeneous, dark grey, silty clay, with minor fine-grained sand component (Owen et al. 1998). <u>Macrofossils:</u> Sediment that contains marine bivalves such as *Crassatella, Ostrea*, or *Tellina* spp. (e.g. Huang et al., 1981).	MTL	<MTL

Sedimentary		Microfossil: Dominance of marine planktonic diatoms such as *Cyclotella striata, Cyclotella comta, Paralia sulcata*, or *Coscinodiscus marginatus* (e.g. Owen et al., 1998; Xiong et al., 2018a).		
	Tidally-influenced environment[1]	**Diagnostic criteria:** Tidal bar to tidal flat: Ripple laminations with bidirectional foreset and cross-laminations dipping approximately 10°, with peaty laminated clay and in-situ bivalves such as *Marctridae* sp. (Tanabe et al., 2003b). Tidal channel: Sediment that contains quartz and feldspar grains and well-rounded calcareous concretions of various sizes, ranging from very coarse sand to pebbles, with oyster fragments (Tanabe et al., 2003a, Tanabe et al., 2003b). Marsh to tidally-influenced channel fill deposit: Sediment with bidirectional ripple cross-laminations with peaty laminated clay with roots (Tanabe et al., 2003b).	<HAT	HAT

	Lagoon deposit	**Diagnostic criteria:** Sedimentary description: Dark grey mud with interbedded thin organic-rich mud and medium to fine sand layers and marine bivalves (Huang et al., 1982; Huang et al., 1986).	HAT	<HAT
	Transgressive contact	**Diagnostic criteria:** Sedimentary description: Transgressive contact between fine to coarse olive grey sand and subangular gravel and overlying marine mud with shell fragments. (e.g. Owen et al., 1998; Cao et al., 2016)	HAT	<HAT
	Alluvial deposit	**Diagnostic criteria:** Sedimentary description: Structureless medium- to coarse-grained sand and rounded gravel, with lenses of clayey silt (Owen et al, 1998) Microfossils: Diatom assemblage characterized by >80% freshwater taxa (Zong, 2013).	MTL	>MTL
	Flood plain	**Diagnostic criteria:** Sedimentary description:	MTL	>MTL

		Grey to yellowish brown clayey silt with herbaceous roots (Fu 2020).		
	Freshwater swamp/ terrestrial peat	**<u>Diagnostic criteria:</u>** <u>Microfossil:</u> Diatom assemblage characterized by >80% freshwater taxa (Zong, 2013; Fu et al., 2020). <u>Macrofossil:</u> Presence of *Glyptostrobus pensilis* (freshwater Pine) wood macrofossils (Huang et al., 1986).	MTL	>MTL
Fixed biological indicator	Relict oyster band on rock faces	**<u>Diagnostic criteria:</u>** <u>Geomorphic feature:</u> Oyster reef remains situated above the intertidal zone, encrusted on rock surface sheltered by overhanging rock slab and is protected from wave action (e.g. Davis et al., 2000). <u>Macrofossil[3]:</u> Oyster remains that are identified to species level (e.g., *Saccostrea cucullata*), with known ecological preference for encrusting habitats within the intertidal zone, where they experience regular submersion and exposure during tidal cycles (Morton and Morton, 1983; Davis et al., 2000)	(181 SWLI + 30 SWLI) /2 OR (MHHW+ MLLW)/2 (in the absence of local surveys)	181 SWLI - 30 SWLI OR MHHW-MLLW (in the absence of local surveys)

	Oyster reef	**<u>Diagnostic criteria:</u>** <u>Macrofossil:</u> Thick accumulation (>0.5 m) of oyster shells (Huang et al., 1981). Common species include *Ostrea (Crassostrea) gigas, Ostrea rivularis,* and *Ostrea denselamellosa*. For example, *C. gigas* is mainly distributed from the low tide line to a water depth of 10 m, with an optimal water depth ranging from 0 to 5 m (Wang, 2008; Wang et al 2023)	MTL	<MTL
Beach	Beach rock	**<u>Diagnostic criteria:</u>** <u>Sedimentary description:</u> Swash zone facies composed of well-sorted sand or shell fragments (shell hash) with plane laminations dipping towards the sea (Tamura, 2012) at an angle between 5–10° (Zong and Li, 1984, Huang, 1992) <u>Petrographic description:</u> Beach rock matrix comprising well-cemented coarse sand with a biolithic component making up 55–65%, primarily bound by calcareous cement. (Yu and Chen, 2009) **<u>Other supporting evidence:</u>** Shell hash that formed the beach facies consists of heterogenous bivalve fossil assemblage (e.g. *Ciree seripta*, *Gefrarium turridum*, *Terebralia* sp., *Ostrea* sp.) (Zhang et al., 1981). Biolithic component including but not limited to fragments of coral, shells, or foraminifera (e.g. Yu	(HAT+LAT)/2	HAT-LAT

		and Chen, 2009). Quartz sand or basalt fragments constitute the remaining components within the matrix (Li, 1988; Huang, 1992).		
Archaeological indicator	Shell midden	**Diagnostic criteria:** Domestic waste composed of bivalve and gastropod shells from fresh and brackish water species. Artifacts such as chipped stones are often found together with shell remains (Huang, 1996). **Other supporting evidence:** Common mollusc species found in the shell midden include *Lamprotula* sp., *Cobicula* sp., *Ostrea* sp., and *Dosinia* sp.	MHHW	>MHHW

[1]Fluvial or channel fill sediments without any supporting evidence on whether sediments were deposited under freshwater or marine conditions (e.g. diatom/foraminifera/bivalve fossils) were rejected as incised channels can form from supratidal to subtidal zone.

The indicative meaning in the table defines the relationship of an indicator to sea level, expressed relative to tidal datums (van de Plassche, 1986; Shennan, 2015). It comprises two components: 1) the indicative range (IR), which represents the 2σ elevation range of the indicator, and 2) the reference water level (RWL), which is the central tendency of its elevation range (Ashe et al., 2022). Indicators that do not form within a precise range relative to sea level but provide upper or lower constraints are classified as marine or terrestrial limiting data points.

For older studies in which conventional ^{14}C ages may not have been corrected for isotopic fractionation, we performed correction for isotopic fractionation (Stuiver and Polach, 1977) using the average 2σ range of the $\delta^{13}C$ of sedimentary facies reported from studies across the SCS (e.g., Yu et al., 2010) or equivalent facies within our RSL database. The corrected ^{14}C uncertainty was calculated as the quadratic sum of analytical measurements, bulk, and isotopic fractionation uncertainty terms (Törnqvist et al., 2015). Corrected ^{14}C ages and uncertainties were calibrated to calendar years using the IOSACAL Python

library (Costa, 2018), which integrates the IntCal20 (Reimer et al., 2020) and Marine20 (Heaton et al., 2020) calibration datasets. For samples determined to form within the marine realm, we estimated the local marine reservoir correction (ΔR) as the weighted mean of ΔR values within a great circle distance of 300 km, with weights determined by the distance from the sample. ΔR values were obtained from the Marine Reservoir Correction database (http://calib.org/marine; Reimer and Reimer, 2001).

Table S5. Screening criteria for classifying samples into two quality levels. Samples classified as L1 satisfied all criteria. Samples were classified as L2 if they met any of the specific criteria related to location, elevation, age, or indicative meaning.

Level	***Screening criteria and examples***	
L1	**Location**	- Sample coordinates were measured (e.g. using Global Positioning System) and reported, or sample location was indicated on a detailed site map.
	Elevation	- The method for measurement of sample elevation (e.g. GNSS RTK system, auto levelling) and the elevation datum (e.g. Hong Kong Principal Datum, Yellow Sea Datum, National Yellow Sea 85 datum) was reported (e.g., Yim, 1999; Xiong et al., 2018a).
	Age	- Description of the dated material was provided. For example, the species name, the condition of the sample (e.g., whether a bivalve was articulated or not), or whether it was a terrestrial or marine taxa was provided.
	Indicative meaning	- The indicator was supported by at least one of the diagnostic criteria listed in Table 1. For example, presence of burrows from bivalves and articulated shells such as *Potamocorbula amurensis* (Asian Brackish-water Clam) and *Corbicula* sp. (e.g., Meacham, 1978) or microfossil assemblages containing 50% brackish benthic diatoms served as diagnostic features for tidal flat facies (e.g., Xiong et al., 2018a).
L2	**Location**	- Sample coordinates were not reported and nor the location of the samples were shown on a map. The relative location of the sample was estimated based on the name of the sample location, for example the name of a village) (e.g., Huang et al., 1983; Huang et al., 1986).
	Elevation	- The sample elevation was not reported, but could be estimated from a digital elevation model (e.g., Li et al., 1991) based on its geographical location. - The reported elevation of a sample was inconsistent between publications. (e.g., Huang et al., 1986; Li et al., 1991).

	Age	- There is evidence that suggests the sample was possibly reworked, such as shell fragments or unarticulated shells dated in a beach rock (e.g. Zhan et al., 1996; Wang, 1998). - Ages reversed in the chronology when there are multiple dates in the same core or site.
	Indicative meaning	- No diagnostic criteria listed in Supplementary table 2 was provided to support the interpretation of the indicator or its indicative meaning (e.g., Huang et al., 1986). For example, a ^{14}C age was reported to be from a tidal flat deposit, but no supporting litho-, bio-, or chemo-stratigraphic information was included in the publication.
L3	**Location**	- The location of the sample could not be reliably estimated to within 2 km.
	Elevation	- The elevation and/or the depth of the sample was not provided, nor could it be reliably estimated from a digital elevation model (e.g., GRI, 1987).
	Age	- The age of the sample was reported as unreliable in original publications (e.g., subject to contamination of older or younger carbon). - Original publications do not include information to recalibrate ^{14}C ages.
	Other	- Insufficient evidence was available to reliably infer a sample's indicative meaning relative to tidal datums.

Screening criteria were applied based on: 1) the reliability of the sample's location, age, and elevation data; and 2) the strength of the supporting evidence for determining each sample's indicative meaning. L2 samples might be influenced by unresolved sources of error that are not fully reflected in the uncertainty estimates listed above, and therefore were not used in the temporal empirical hierarchical (ET-GP) model (Figure 8). For instance, reworked shell in beach deposit only provides a maximum age constraint on RSL and its 2σ age uncertainty, and might not accurately represent the timing of its true RSL position in the past. We also considered as L2 if it was reported to have formed in a specific environment without any supporting evidence (i.e., the diagnostic criteria listed in Supplementary table 2). L3 samples are those for which the location, age, elevation, or indicative meaning could not be reasonably estimated, and were excluded from further analysis.

Figure S5. All Holocene sea-level index points of Hong Kong and the PRD from 12 ka to present day. The type of RSL data (index point and limiting point) is denoted by symbol and colour. L2 indicators are shown with half transparency. Intercalated samples are outlined by black boxes. The grey envelope represents the ±1σ confidence interval of RSL predictions derived from the ET-GP, applied only to the highest quality L1 data. The red envelope represents the ±1σ confidence interval of RSL predictions applied to both L1 and L2 data. Only limiting points constraining RSL are shown in the figure.

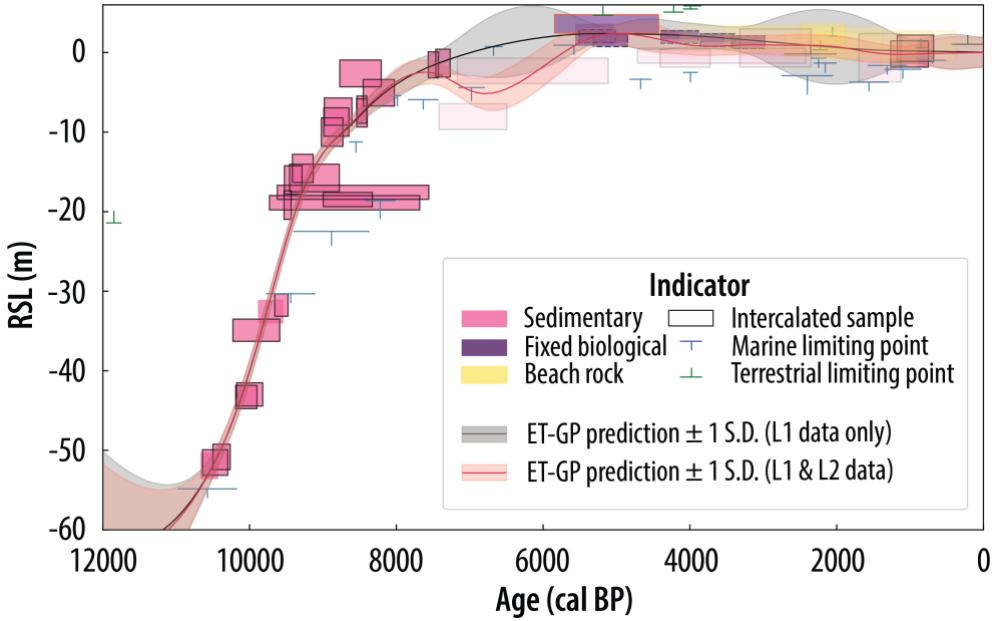

Table S6. Hyperparameter settings for the ET-GP applied to RSL data compiled from far-field locations.

Site	***Amplitude (m)***	***Time scale (ka)***	***White noise (m)***
St. Croix	104	27.1	1.4
Suriname and Guayana	115.5	27.7	0.9
Natal, Brazil	124.3	30.2	0.9
Tunisia	104.4	24.4	0.7
South Africa	97.9	22.3	1.3
Hong Kong and Pearl River Delta, China (L1 data only)	33.5	4.9	2
Hong Kong and Pearl River Delta, China (L1 and L2 data)	35	5.2	2
Singapore	91.6	21.6	1.1
North Queensland, Australia	51.2	2	0.4
New South Wales, Australia	67.1	11.9	0.002

Supplementary reference

Ashe, E. L., Khan, N. S., Toth, L. T., Dutton, A., & Kopp, R. E. (2022). A statistical framework for integrating nonparametric proxy distributions into geological reconstructions of relative sea level. Advances in Statistical Climatology, Meteorology and Oceanography, 8(1), 1-29.

Cao, X., Yin, Y., Jia, P., & Li, X. A. (2016). Sedimentary records and environmental revolution of the core LDB01in Lingshui County, Hainan. Quaternary Sciences, 36(1), 31-43 (In Chinese).

Carlton, J. T., Tompson, J. K., Schemel, L. E., & Nichols, F. H. (1990). Remarkable invasion of San Francisco Bay (California, USA), by the Asian clam Potamocorbula amurensis. I. Introduction and dispersal. Marine Ecology Progress Series, 66, 81-94.

Costa, S., 2018. IOSACal: v0.4.0.

Davis, A., Aitchison, J., Flood, P., Morton, B., Baker, R., & Haworth, R. (2000). Late Holocene higher sea-level indicators from the South China coast. Marine Geology, 171(1-4), 1-5.

Fu, S., Xiong, H., Zong, Y., & Huang, G. (2020). Reasons for the low sedimentation and slow progradation in the Pearl River delta, southern China, during the middle Holocene. Marine Geology, 423, 106133.

Heaton, T. J., Köhler, P., Butzin, M., Bard, E., Reimer, R. W., Austin, W. E., Ramsey, R. W., Grootes, P. M., Hughen, K. A., Kromer, B., Reimer, P.J., Adkins, J., Burke, A., Cook, M. S., Olsen, J., & Skinner, L. C. (2020). Marine20—the marine radiocarbon age calibration curve (0–55,000 cal BP). Radiocarbon, 62(4), 779-820.

Hori, K., Tanabe, S., Saito, Y., Haruyama, S., Nguyen, V., & Kitamura, A. (2004). Delta initiation and Holocene sea-level change: example from the Song Hong (Red River) delta, Vietnam. Sedimentary Geology, 164(3-4), 237-249.

Huang Y., Xia F., Huang D. (1981). Holocene sea level changes and crustal movements along coastal zones of the northern South China Sea. Acta Oceanol Sin, 4(6): 713–723 (in Chinese).

Huang, Z., Li, P., Zhang, Z., Li, K., Qiao, P., (1982). Zhujiang (Pearl) Delta. General Scientific Press, Guangzhou (in Chinese).

Huang, Z., Li, P., Zhang, Z., Li, K., Qiao, P., Zong, Y. (1983). The Landforms of Shenzhen. Guangdong Scientific and Technological Press (In Chinese).

Huang, Z., Li, P., Zhang, Z., & Zong, Y. (1986). Changes of sea level in south China coast since the Late Pleistocene. China Sea-level Changes, 178-194 (In Chinese).

Huang, Z. (1992). Comparison of beach rock between China and Japan. Tropical Geography, 12(2): 108-121 (in Chinese).

Huang, G. (1996). Neolithic culture and paleogeographic environment in the Zhujiang Delta. Acta Geographica, 51, 517-525 (in Chinese).

Li, P. (1988). Holocene beachrock in South China and its paleogeographic significance. Marine Geology and Quaternary Geology, 8(4), 21-29 (in Chinese).

Li, P., Qiao, P., Zheng, H., Fang, G., Huang, G., (1991). Environmental evolution of Zhujiang Delta in the Past 10000 years. China Ocean Press, Beijing, 154pp. (in Chinese).

Meacham, W. (1978). Sham Wan, Lamma Island: an archaeological site study. Hong Kong Archaeological Society.

Morton, B., Morton, J., (1983). The Sea Shore Ecology of Hong Kong. Hong Kong University Press, Hong Kong (350pp.).

Owen, R. B., Neller, R. J., Shaw, R., & Cheung, P. C. T. (1998). Late Quaternary environmental changes in Hong Kong. Palaeogeography, Palaeoclimatology, Palaeoecology, 138(1-4), 151-173. https://doi.org/10.1016/s0031-0182(97)00129-6

Reimer, P. J., & Reimer, R. W. (2001). A marine reservoir correction database and on-line interface. Radiocarbon, 43(2A), 461-463.

Reimer, P.J., Austin, W.E.N., Bard, E., Bayliss, A., Blackwell, P.G., Bronk Ramsey, C., Butzin, M., Cheng, H., Edwards, R.L., Friedrich, M., Grootes, P.M., Guilderson, T.P., Hajdas, I., Heaton, T.J., Hogg, A.G., Hughen, K.A., Kromer, B., Manning, S.W., Muscheler, R., Palmer, J.G., Pearson, C., van der Plicht, J., Reimer, R.W., Richards, D.A., Scott, E.M., Southon, J.R., Turney, C.S.M., Wacker, L., Adolphi, F., Büntgen, U., Capano, M., Fahrni, S.M., Fogtmann- Schulz, A., Friedrich, R., K¨ohler, P., Kudsk, S., Miyake, F., Olsen, J., Reinig, F., Sakamoto, M., Sookdeo, A., Talamo, S., 2020. The IntCal20 Northern Hemisphere radiocarbon age calibration curve (0–55 cal kBP). Radiocarbon 62, 725–757.

Shennan, I. (2015). Handbook of sea-level research: framing research questions. Handbook of sealevel research, 3-25.

Stuiver, M., & Polach, H. A. (1977). Discussion reporting of 14C data. Radiocarbon, 19(3), 355-363.

Sun, Y., Xiong, H., Lee, M. T., Brodie, C., & Zong, Y. (2021). Geochemical dynamics and depositional history from mangrove sediments within the Pearl River estuary. Palaeogeography, Palaeoclimatology, Palaeoecology, 584, 110701.

Tamura, T. (2012). Beach ridges and prograded beach deposits as palaeoenvironment records. Earth-Science Reviews, 114(3-4), 279-297

Tanabe, S., Hori, K., Saito, Y., Haruyama, S., & Kitamura, A. (2003a). Song Hong (Red River) delta evolution related to millennium-scale Holocene sea-level changes. Quaternary science reviews, 22(21-22), 2345-2361.

Tanabe, S., Hori, K., Saito, Y., Haruyama, S., Sato, Y., & Hiraide, S. (2003b). Sedimentary facies and radiocarbon dates of the Nam Dinh-1 core from the Song Hong (Red River) delta, Vietnam. Journal of Asian earth sciences, 21(5), 503-513.

Tanabe, S., Saito, Y., Vu, Q. L., Hanebuth, T. J., Ngo, Q. L., & Kitamura, A. (2006). Holocene evolution of the Song Hong (Red River) delta system, northern Vietnam. Sedimentary Geology, 187(1-2), 29-61.

Törnqvist, T. E., Rosenheim, B. E., Hu, P., & Fernandez, A. B. (2015). Radiocarbon dating and calibration. Handbook of Sea-Level Research, 347-360.

Van de Plassche, O., (1986). Introduction. In: Sea-Level Research: A Manual for the Collection and Evaluation of Data. Geobooks, Norwich.

Wang, W. (1998). Beach rocks and storm deposits on the beaches of Hong Kong. Science in China Series D: Earth Sciences, 41(4), 369-376.

Wang, H., Zhang, G., Liu, X., & Guo, X. (2008). Classification of common oysters from North China. Journal of Shellfish Research, 27(3), 495-503.

Wang, X., Zhang, J., Zhong, Y., Liu, Y., & Wu, W. (2023). GIS-based spatial suitability assessment for pacific oyster Crassostrea gigas reef restoration: A case study of Laizhou Bay, China. Marine Pollution Bulletin, 186, 114416

Xia, P., Meng, X., Li, Z., Zhi, P., Zhao, M., & Wang, E. (2019). Late Holocene mangrove development and response to sea level change in the northwestern South China Sea. Acta Oceanologica Sinica, 38(11), 111-120.

Xiong, H., Zong, Y., Qian, P., Huang, G., & Fu, S. (2018a). Holocene sea-level history of the northern coast of South China Sea. Quaternary Science Reviews, 194, 12-26.

Xiong, H., Zong, Y., Huang, G., & Fu, S. (2018b). Sedimentary responses to Holocene sea-level change in a shallow marine environment of southern China. Journal of Asian earth sciences, 166, 95- 106.

Xiong, H., Zong, Y., Huang, G., Fu, S., 2020. Seabed erosion and deposition related to the typhoon activity of the past millennium on the southeast coast of China. Earth Surf. Process. Landf. 45, 1695–1704.

Xu, J. L. (1985). Shoal Growth and Evolution of Lingdingyang of the Pearl River Mouth (In Chinese).

Yim, W. W. S. (1999). Radiocarbon dating and the reconstruction of late Quaternary sea-level changes in Hong Kong. Quaternary International, 55(1), 77-91.

Yu, K., & Chen, T., C. (2009). Beach sediments from northern South China Sea suggest high and oscillating sea levels during the late Holocene. Earth Science Frontiers, 16(6), 138-145.

Yu, F., Zong, Y., Lloyd, J. M., Huang, G., Leng, M. J., Kendrick, C., Lamb, A. L.. & Yim, W. W. S. (2010). Bulk organic δ13C and C/N as indicators for sediment sources in the Pearl River delta and estuary, southern China. Estuarine, Coastal and Shelf Science, 87(4), 618-630.

Yu, H. K., Khan, N. S., Desianti, N., Garrett, E., Planavsky, N. J., & Ahmed, A. (2025). The utility of mangrove foraminifera, diatoms, and stable carbon isotope and C/N geochemistry in relative sea-level reconstruction in the Pearl River Delta, China. Marine Geology, 107610.

Zhan, W., Liu, Y., Zhong, J. (1996). Discussion on historical sea level changes based on beachrocks along coast of Guangdong. South China Sea Research and Exploration, 4, 30–35 (In Chinese).

Zhang, J., Li, G., & Zhao, X. (1981). The age of formation of the marine shells and beach rocks in the Yinggehai region, Hainan Island. Seismology and Geology, 3(1), 66 (In Chinese).

Zhang, H., Huang K., Chen, G., Li, Z., Chen, W., Zhang, J., & Zhao, X. (1982). On the Remnant of Ancient Marine Erosion in the Sheji Area, Nanhai County, Guangdong. Marine Sciences, 1, 12–16 (In Chinese).

Zheng, Z., & Li, Q. (2000). Vegetation, climate, and sea level in the past 55,000 years, Hanjiang Delta, Southeastern China. Quaternary Research, 53(3), 330-340.

Zong, Y. & Li, P. (1984). Analysis of condition to form the Holocene beachrock along the coast of eastern Guangdong. Tropical Geography, 4(4), 205-212 (In Chinese).

Zong, Y., Zheng, Z., Huang, K., Sun, Y., Wang, N., Tang, M., & Huang, G. (2013). Changes in sea level, water salinity and wetland habitat linked to the late agricultural development in the Pearl River delta plain of China. Quaternary science reviews, 70, 145-157.